DEVELOPMENT OF NOVEL DATA PROCESSING SCHEMES AND GLOBAL SEISMIC EVENT DATABASE AND SPECIAL STUDIES TO SUPPORT THE EXPLOSIONS MONITORING RESEARCH PROGRAM

Patricia Doherty, et al.

Boston College
Institute for Scientific Research
140 Commonwealth Avenue
Chestnut Hill, MA 02467

28 June 2012

Final Report

APPROVED FOR PUBLIC RELEASE; DISTRIBUTION IS UNLIMITED.

AIR FORCE RESEARCH LABORATORY
Space Vehicles Directorate
3550 Aberdeen Ave SE
AIR FORCE MATERIEL COMMAND
KIRTLAND AIR FORCE BASE, NM 87117-5776

DTIC COPY

NOTICE AND SIGNATURE PAGE

Using Government drawings, specifications, or other data included in this document for any purpose other than Government procurement does not in any way obligate the U.S. Government. The fact that the Government formulated or supplied the drawings, specifications, or other data does not license the holder or any other person or corporation; or convey any rights or permission to manufacture, use, or sell any patented invention that may relate to them.

This report was cleared for public release by the 377 ABW Public Affairs Office and is available to the general public, including foreign nationals. Copies may be obtained from the Defense Technical Information Center (DTIC) (http://www.dtic.mil).

AFRL-RV-PS-TR-2012-0122 HAS BEEN REVIEWED AND IS APPROVED FOR PUBLICATION IN ACCORDANCE WITH ASSIGNED DISTRIBUTION STATEMENT.

//SIGNED//   //SIGNED//

_____   _____
    Robert Raistrick   Joel B. Mozer
    Program Manager, RVBYE   Chief, AFRL/RVB

This report is published in the interest of scientific and technical information exchange, and its publication does not constitute the Government's approval or disapproval of its ideas or findings.

REPORT DOCUMENTATION PAGE

1. REPORT DATE *(DD-MM-YYYY)* 28-06-2012	2. REPORT TYPE Final Report	3. DATES COVERED *(From - To)* 12 Jan 2007 – 30 Apr 2012

4. TITLE AND SUBTITLE

Development of Novel Data Processing Schemes and Global Seismic Event Database and Special Studies to Support the Explosions Monitoring Research Program

5a. CONTRACT NUMBER
FA8718-06-C-0075

5b. GRANT NUMBER

5c. PROGRAM ELEMENT NUMBER
62601F

6. AUTHOR(S)

Patricia Doherty[1], Jessie Bonner[2], Delaine Reiter[2], Estela Minaya[3], Mario Zabala[3] and Maracia Antelo[3]

5d. PROJECT NUMBER
1010

5e. TASK NUMBER
PPM00004172

5f. WORK UNIT NUMBER
EF004620

7. PERFORMING ORGANIZATION NAME(S) AND ADDRESS(ES)

Boston College
Institute for Scientific Research
140 Commonwealth Avenue
Chestnut Hill, MA 02467

8. PERFORMING ORGANIZATION REPORT NUMBER

9. SPONSORING / MONITORING AGENCY NAME(S) AND ADDRESS(ES)
Air Force Research Laboratory
Space Vehicles Directorate
3550 Aberdeen Ave. SE
Kirtland AFB, NM 87117-5776

10. SPONSOR/MONITOR'S ACRONYM(S)

AFRL/RVBYE

11. SPONSOR/MONITOR'S REPORT NUMBER(S)

AFRL-RV-PS-TR-2012-0122

12. DISTRIBUTION / AVAILABILITY STATEMENT

Approved for Public Release; Distribution is unlimited. (377ABW-2012-0755 dtd 21 June 2012)

13. SUPPLEMENTARY NOTES
[1]Boston College, Chestnut Hill, MA
[2]Weston Geophysical Corporation, Lexington, MA
[3]Observatorio San Calixto, La Paz, Bolivia

14. ABSTRACT

The Boston College Institute for Scientific Research (ISR) has conducted innovative research using tools, analysis techniques, and database development to support the Air Force Research Laboratory's (AFRL) nuclear monitoring program. The innovative research objectives of this task have been directed toward applying waveform modeling techniques to earthquakes and explosions at locations of interest to the community where both teleseismic and regional waveform data are available. Moderate to large earthquake sources provide high resolution ground truth information for regional studies of earthquake and explosion phenomenology. Some of our major efforts included the New England Damage Experiment where the question of shear wave generation mechanisms for explosive sources was addressed. Another major effort included the determination of attenuation parameters in La Paz, Bolivia for improved seismic phase identification.

15. SUBJECT TERMS
Waveform modeling, Shear wave generation, Seismic phase identification

16. SECURITY CLASSIFICATION OF:			17. LIMITATION OF ABSTRACT	18. NUMBER OF PAGES	19a. NAME OF RESPONSIBLE PERSON Robert Raistrick
a. REPORT Unclassified	**b. ABSTRACT** Unclassified	**c. THIS PAGE** Unclassified	Unlimited	42	**19b. TELEPHONE NUMBER** *(include area code)*

This page is intentionally left blank.

TABLE OF CONTENTS

List of Figures

List of Tables

This page is intentionally left blank.

1. INTRODUCTION

The innovative research objectives of this task have been directed toward applying waveform modeling techniques to earthquakes and explosions at locations of interest to the community where both teleseismic and regional waveform data are available. Moderate to large earthquake sources provide high resolution ground truth information for regional studies of earthquake and explosion phenomenology. Some of our major efforts included the New England Damage Experiment where the question of shear wave generation mechanisms for explosive sources was addressed. Another major effort included the determination of attenuation parameters in La Paz, Bolivia for improved seismic phase identification.

All of the research efforts were performed by Boston College personnel together with subcontracts awarded to Weston Geophysical Corporation of Lexington, MA and the Observatorio San Calixto in La Paz, Bolivia.

2. NEW ENGLAND DAMAGE EXPERIMENT

2.1 BACKGROUND

The New England Damage Experiment (NEDE) addresses the question of shear wave generation mechanisms for explosive sources. The purpose of the experiment is to generate different types of fractures in a homogeneous source medium, examine the phases generated at a range of distances, and compare the phase generation with the source rock damage. S-wave generation has been predicted in the far field as a result of crack growth [1], and the cone of damage above a source has been shown to be responsible for generating *Rg* in the near field [2] and *S(Lg)* in the far field [3,4]. This experiment will provide empirical data to further illuminate the mechanisms of shear wave generation.

Five shots of three different explosives were detonated at the Rock of Ages Quarry in Barre, VT in homogeneous, low-fracture density granite. The three types of explosives have different velocities of detonation (VOD). Fast VOD explosives pulverize the surrounding material quickly and prevent explosive gases from getting into cracks in the rock. Damage near the blast is great, but individual cracks are not very large, nor do they propagate very far. Slow VOD explosives allow explosive gases to get into cracks, resulting in bigger, longer cracks. Two linear arrays and a near-source array were deployed specifically for this experiment. The linear arrays extend radially for about 30 km to the NE and SE of the shot locations, and consist of short-period, three component seismometers spaced every 3 km, and 4.5 Hz, vertical single component Texans every 0.5 km (see Figure 1). The near-source array consists of both Texans and three component seismometers and accelerometers (see Figure 2), but for the purposes of this part of the study, only the circular Texans are used to examine anisotropy near the source. These circular Texans were deployed in a ring about 0.5-1 km away from the blasts, and will be useful in determining radiation patterns and the effects of anisotropy. Borehole cores from the test site were taken both before and after the blasts to examine rock damage and to quantify properties of the Barre granite. Velocities of the core samples were measured by New England Research, Inc., and the granite was found to have strong anisotropy, with velocity ranging from about 4.6 km/s at an azimuth of 30° to 3.8 km/s at 120°.

2.2 METHODS, ASSUMPTIONS AND PROCEDURES

A brief overview of the moment tensor inversion is given here; for a more complete description, see [5]. Moment tensors were calculated for the five shots using five of the near-source, three-component instruments. An accurate velocity model is a critical component of a moment tensor inversion. A 1D velocity model was developed for the upper 100 m using the core sample velocities and seismic refraction travel-time data from the near-source instruments. While the resulting moment tensors do have dominant diagonal components, there is significant energy on the off-diagonals as well. Some phases, such as *Rg,* are not well-fit by the Green's functions used in the moment tensor inversion. Because the velocity model controls the goodness of fit of the Green's functions to the data, a more accurate velocity model should be able to improve these fits, and in turn, improve the moment tensors. Additionally, an accurate velocity model for the entire region, rather than just the near source, will allow many more stations to be included in the moment tensor inversion. Developing this 3D velocity model is the aim of this part of the study.
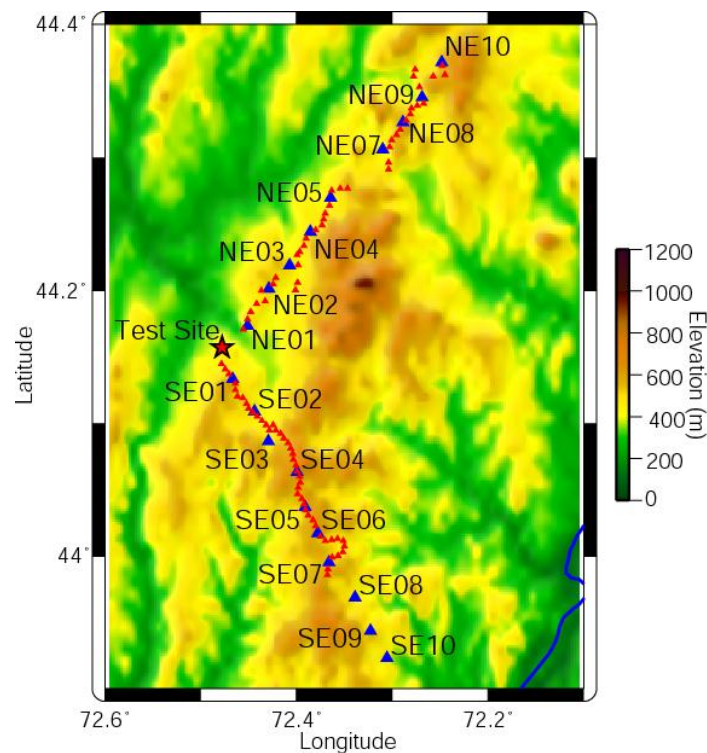
Figure 1. Map of NE and SE Linear Arrays

(Texans depicted with red triangles and short period-three component instruments depicted with blue triangles).

2
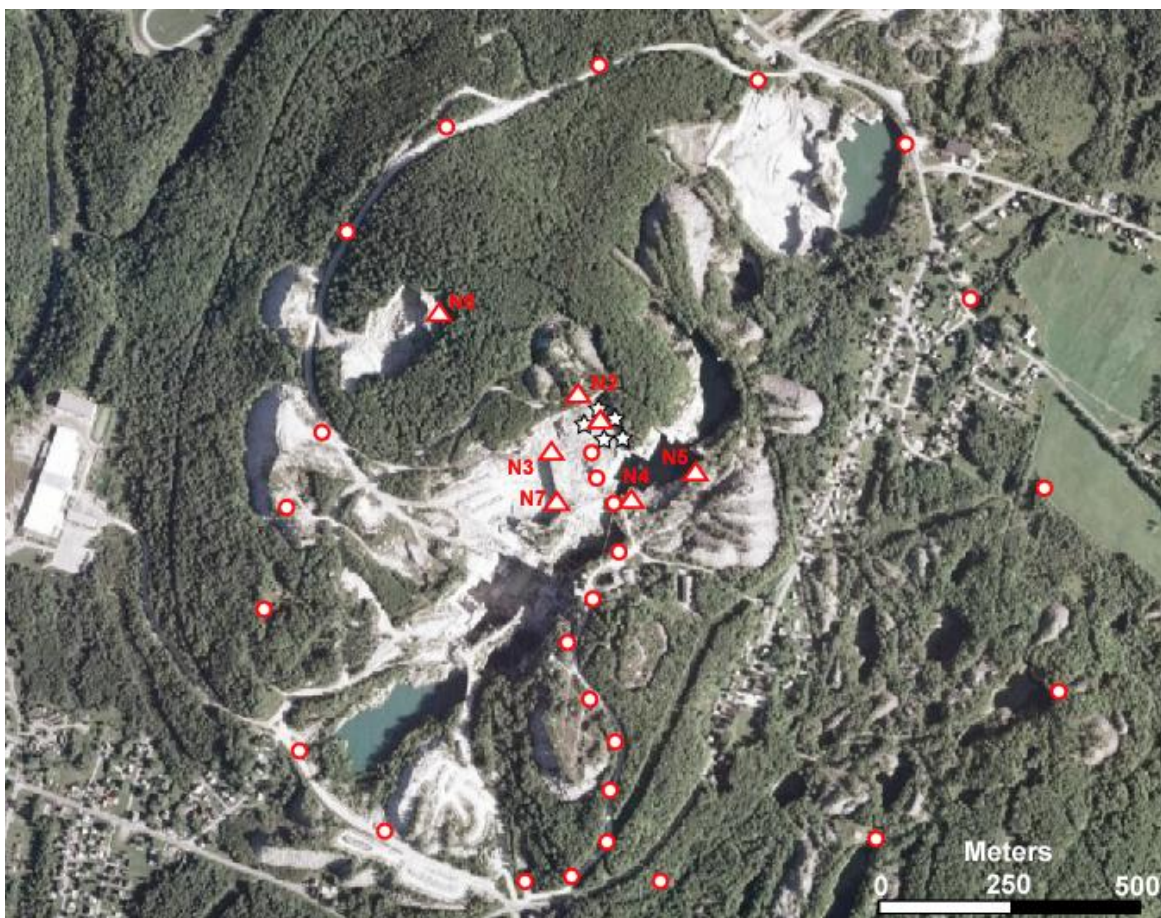
Figure 2. Map of the Blast Area and Near-Source Instruments

(The shots are shown as stars, three-component, short-period instruments are triangles, and vertical-component Texans are circles. In this velocity model study, only the circular Texans, those deployed in a ring around the blast site, are used.)

P-wave Velocity Model

We have completed a P-wave velocity model for the region using seismic refraction profiles. We picked first arrivals for all data and performed static elevation corrections. Elevation differences were all less than 200 m, and the largest time correction was 0.02 s. For the NE and SE lines, we analyzed travel time vs. distance curves (Figure 3). The NE line refraction profile suggests a single layer with a velocity of 6.1 km/s. The profile for the SE line reveals two layers with velocities of 5.5 and 6.0 km/s.

NEDE Refraction Profile, NE line

NEDE Refraction Profile, SE line
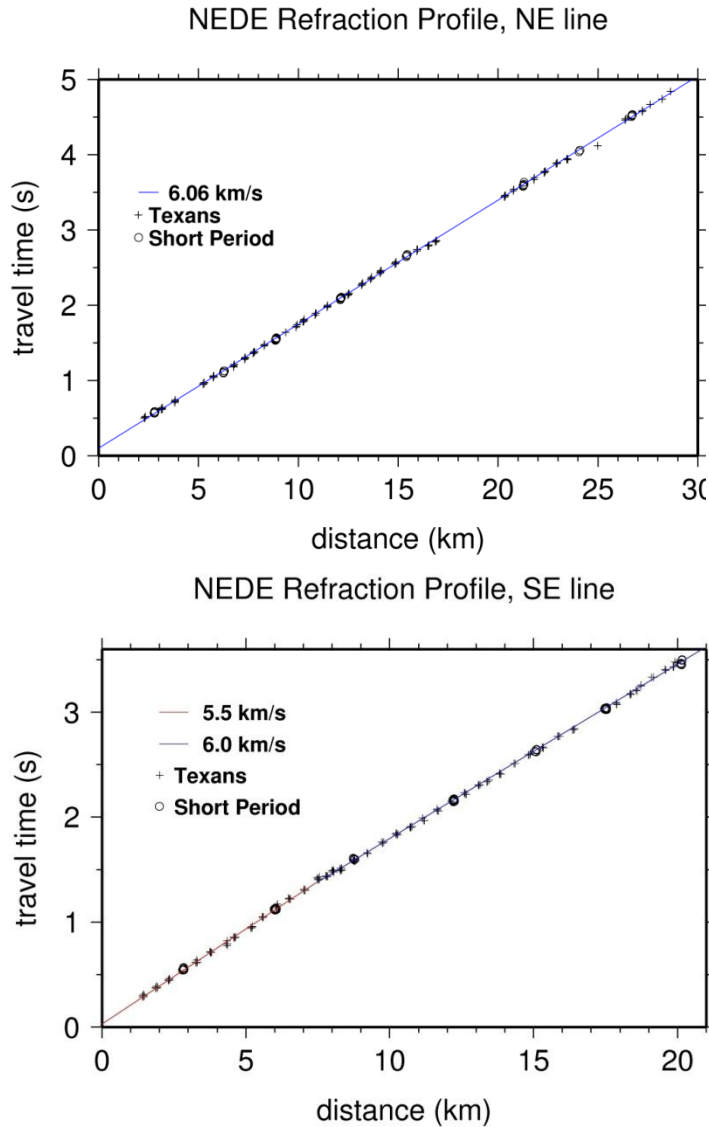
Figure 3. Refraction Profiles for the NE and SE Linear Arrays

(The NE line (above) has a constant slope, indicating a single layer with a constant velocity. The SE line (below) has a break in slope, indicating two-layer model.)

S-wave Velocity Model

Rg dispersion curves were estimated for short-period and Texan data on the NE and SE lines using CPS do_mft. For each line, dispersion curves were averaged for all stations and all shots, using the maximum amount of data for each average. The average curves with one standard deviation error bars are show in Figure 4. A starting shear velocity model was estimated from the results of the P-wave velocity model using a Vp/Vs ration of 1.9.

To reduce the final model's dependence on the starting model, we performed a stochastic inversion. The starting model was divided into 10 layers of 0.1 km thickness each, all over a halfspace. Then we generated a new starting model by randomly perturbing each layer by -10 to 10%. We generated 300 of these perturbed models, ran five iterations of each one, resulting in 300 intermediate models. The final model is the mean of each layer of the 300 intermediate

4

models. Figure 5 shows the starting model in blue, the limits of the random perturbations as blue dashed lines, the intermediate models in gray, the final model in red, and the standard deviation of the mean as red dashed lines.
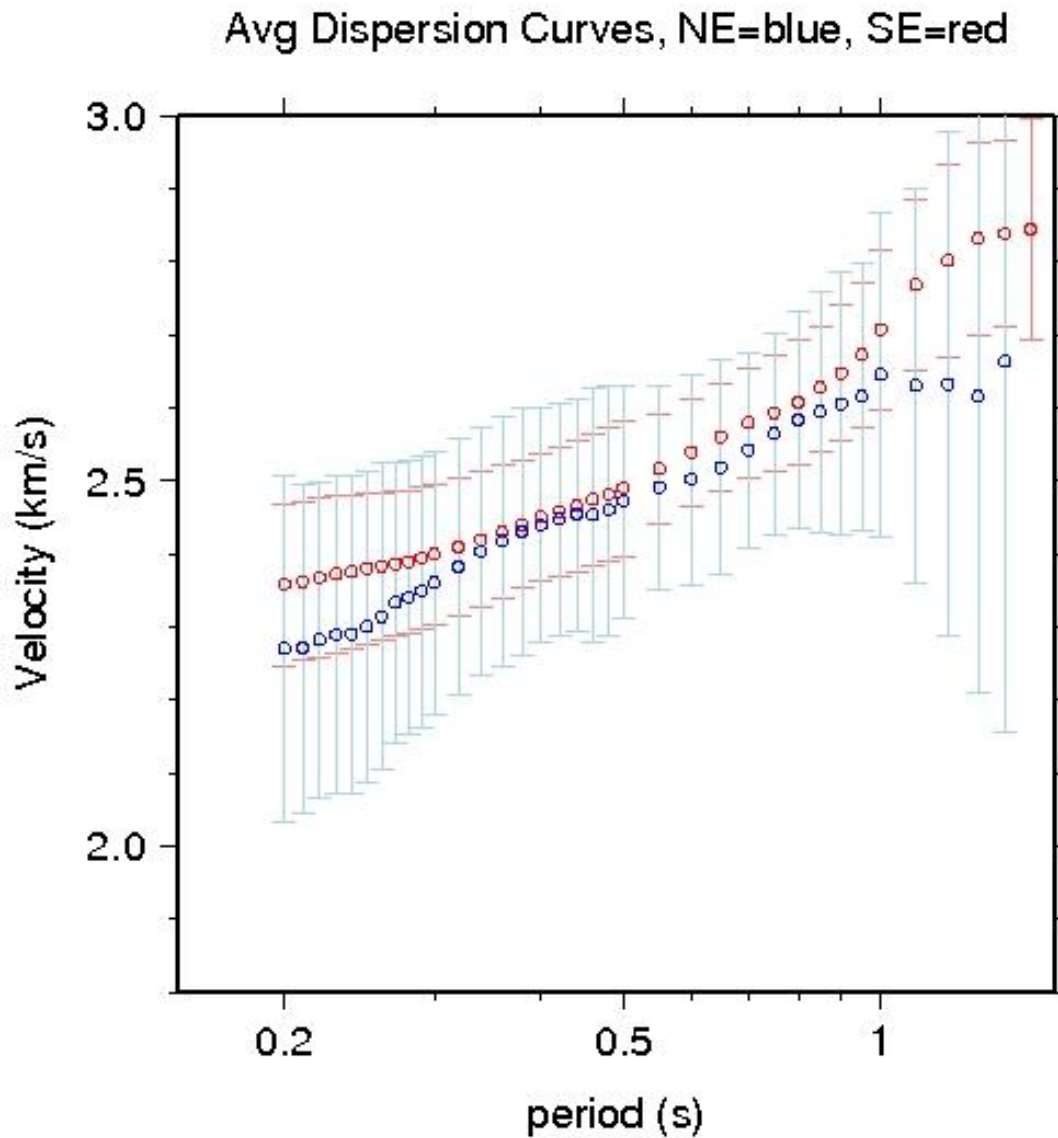
Figure 4. Average Dispersion Curves for the NE and SE Lines

(The average includes all shots and all stations for each line. Error bars represent standard deviation. The NE line is in blue and the SE in red).
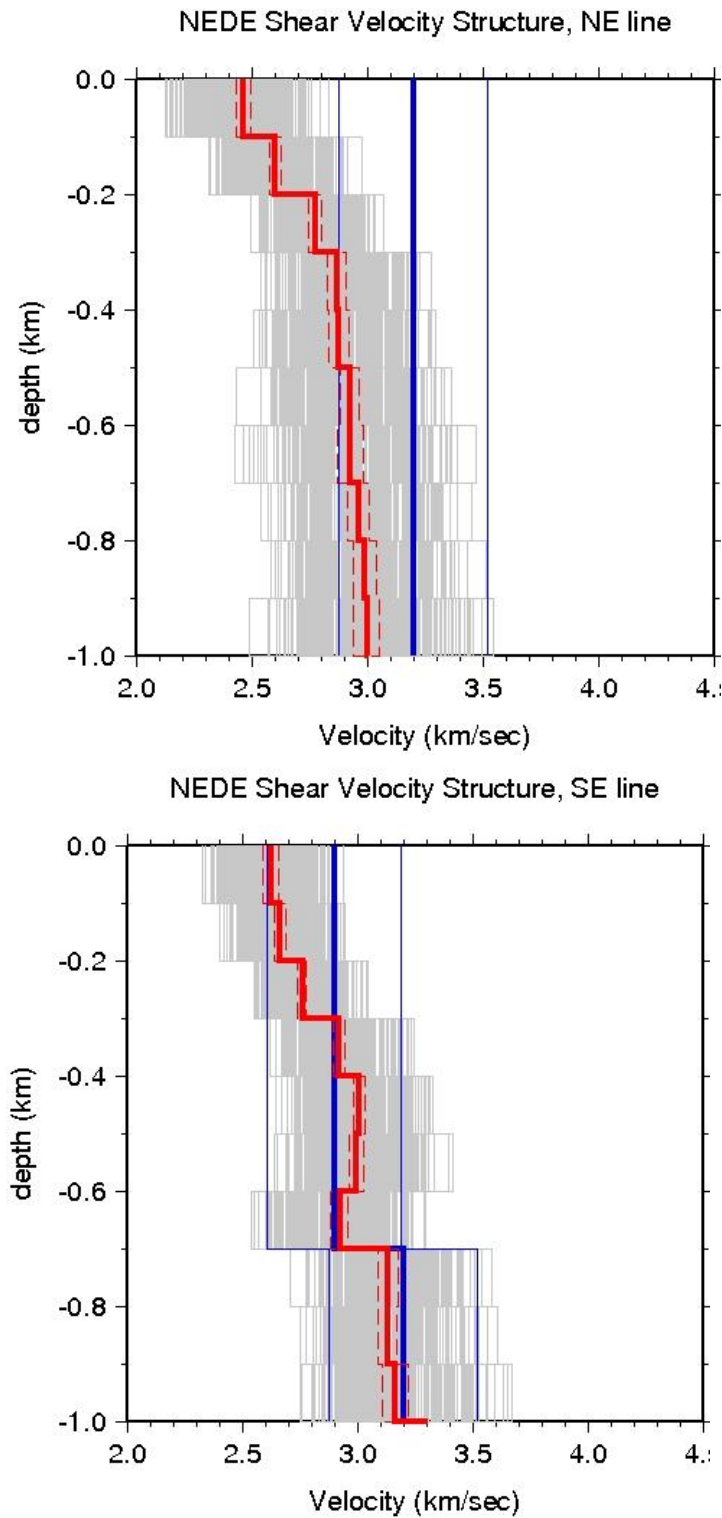
Figure 5. Final Velocity Models for the NE and SE Lines

(The thick blue line is the starting velocity model derived from the P-wave refraction study, think blue lines are the limits of the random perturbations for the stochastic inversion, gray lines are the intermediate models, red thick line is the mean of the gray lines, or final model, and red dashed lines are the standard deviation of the mean).
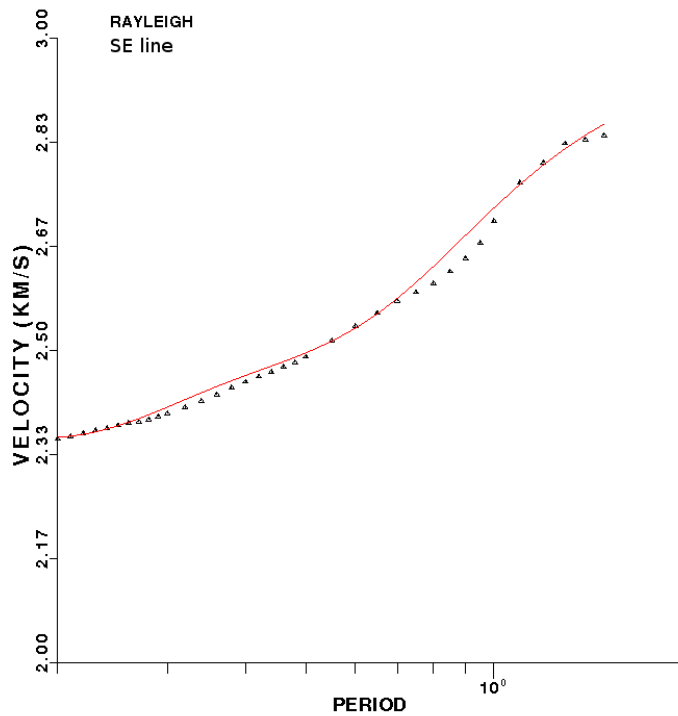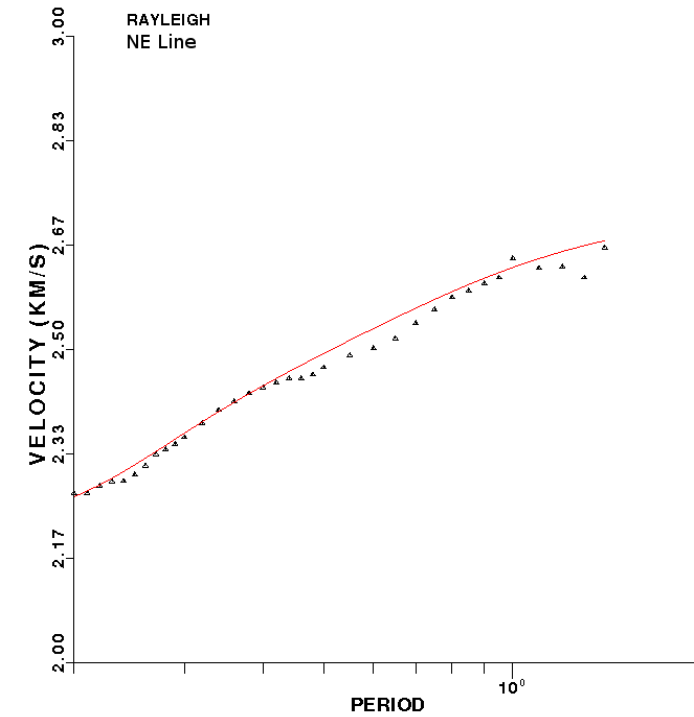
Figure 6. Average Dispersion Curves and Calculated Dispersion Curves from the Velocity Models

(Dispersion curves represented with dots and calculated dispersion curves with red lines).

7

Lateral Velocity Changes

Next, we investigate the possibility of velocity variations along the length of the profiles. We plot dispersion curves for all shots and all short period stations, color coded by distance in bins of 5 km (Figure 7). Colors are in rainbow order, with red representing distances greater than 25 km, and purple less than 5 km. From this preliminary analysis, it does appear that the SE line is faster at greater distances, while the SE line is less clear. We perform a differential velocity model inversion to try to quantify these lateral velocity changes.
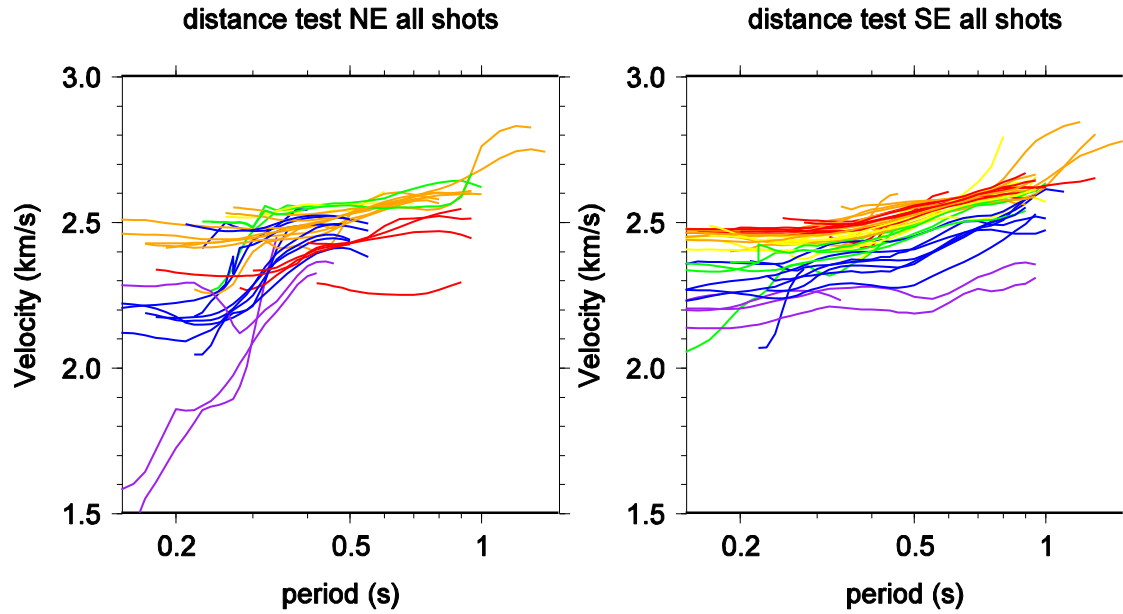
Figure 7. Short-Period Dispersion Curves

(Curves colored by distance. Red >=25 km, 25<Orange<20, 20<Yellow<15, 15<Green<10, 10<blue<5, Purple<=5. The NE line does not show strong differences in velocity with distance, especially beyond 10 km. The SE line, however, shows an increase in velocity with distance away from the source).

Differential Shear-Wave Velocity Model Inversion

We perform a differential inversion by calculating the dispersion curve contribution between short-period stations along the SE line and performing velocity model inversions for these new curves. First, we average the dispersion curves over the different shots at each station. Then we calculate the group velocity curve, *D(T)* at each station *N*:

$$D_N(T) = \frac{dist_N}{U(T)}$$

(1)

where *U(T)* is the group velocity curve at station *N* for all periods *T*. $D_N(T)$ is equivalent to the period-dependent Rayleigh-wave travel time at each station. We then calculate the difference in group velocity curves between adjacent stations to find the group delay, *G(T)*

$$G(T) = D_{N+1}(T) - D_N(T) \qquad (2)$$

In calculating the group delay, we use stations with a minimum separation distance of 3 km to avoid negative group delays that can result from more closely-spaced stations. Finally we can calculate the differential dispersion curve, $U_d(T)$:

$$U_d(T) = \frac{dist_{N+1} - dist_N}{G(T)} \qquad (3)$$

2.3 RESULTS AND DISCUSSION

The results of this inversion for the SE line are in Figure 8. The starting velocity model (blue line) and model resulting from the differential inversion (red line) are shown in the panel on the left. On the right are the averaged interstation dispersion curves (black triangles) and the calculated ones (red line) corresponding to the final velocity model. These results are very preliminary and the question of lateral velocity changes requires more extensive study. We can conclude that for the SE line at least, velocity does appear to increase with distance away from the shot. The NE line is unclear. This differential inversion is a first step in quantifying these velocity differences. Unfortunately, we have gone as far as we can in this study, at this time.
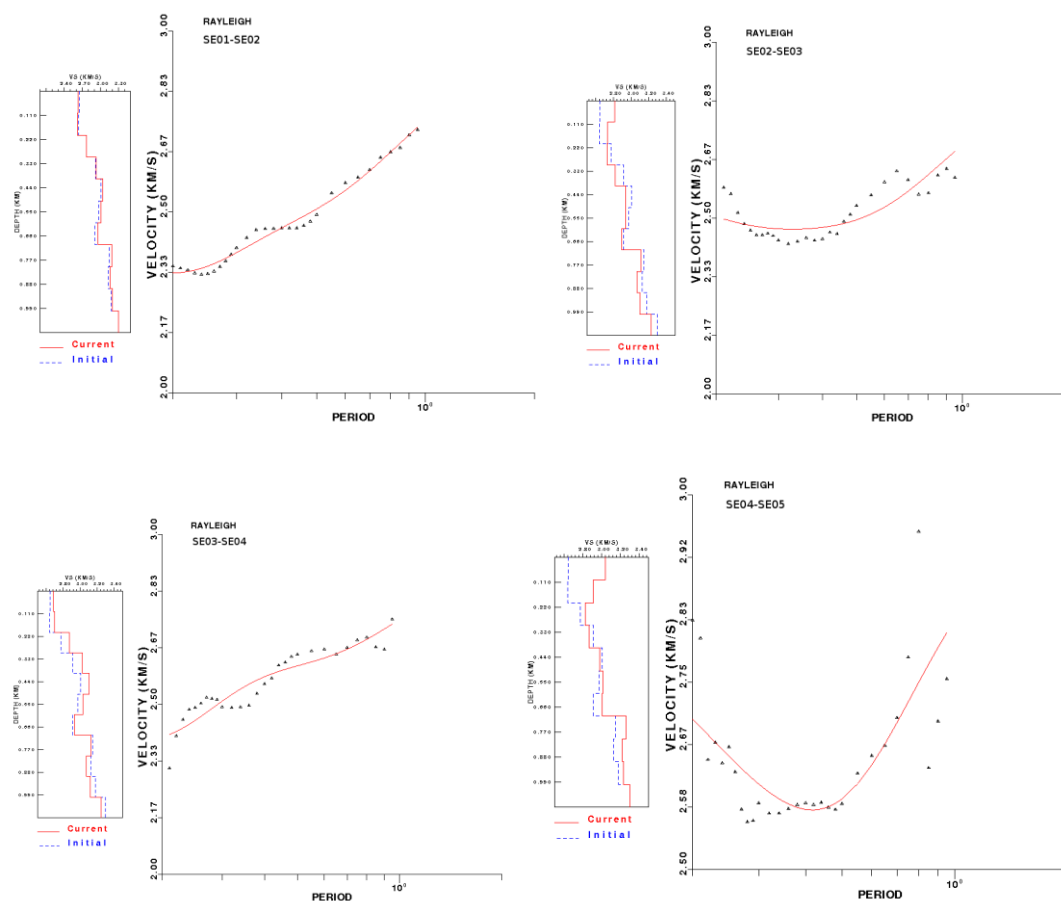
(See Figure 8 caption on the next page).

Approved for Public Release; Distribution is unlimited.
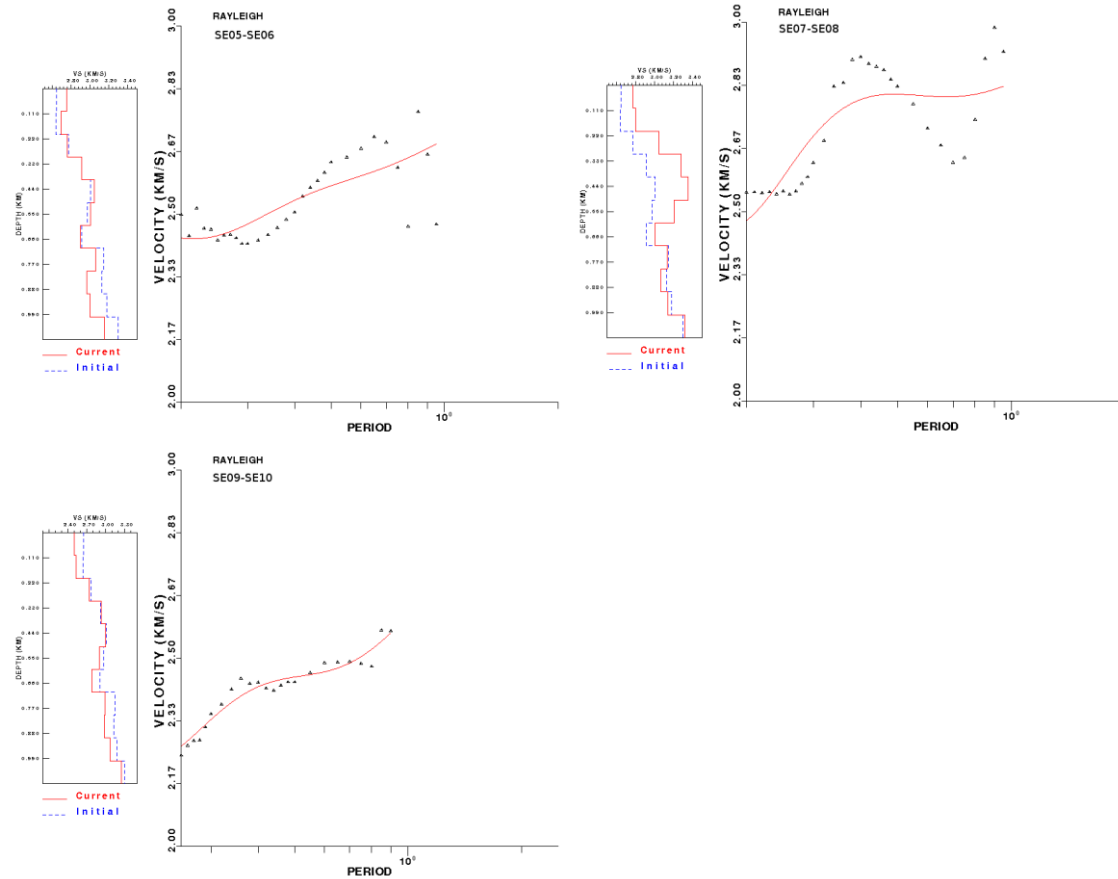
Figure 8. Differential Velocity Model and Dispersion Curve Results for Select Station Pairs

(In the left panel, the initial velocity model (dashed blue line) and model calculated in the differential inversion (red line) are shown. The averaged interstation dispersion curve is shown as black triangles, and the red line is the dispersion curve resulting from the differential inversion. For each interstation distance, there is a velocity model and dispersion curve.)

Near-Source Anisotropy

We expect to see anisotropy with a fast direction oriented at approximately 30°, as was found in the core samples taken from the blast site. Our results from the seismic data suggest that there may be some anisotropy, but it does not appear as strong as in the core samples.

The slightly faster velocities on the NE line compared to the SE line are in agreement with the fast direction of 30° found in the core samples, but the anisotropy is less pronounced. However, the azimuths of the NE and SE lines, 40° and 153°, respectively, are off-strike from the fast and slow directions of the core sample (30° and 120°), so the difference in velocities may be under-representative of the true anisotropy of the region.

10

NEDE Circular Texan P-wave velocities
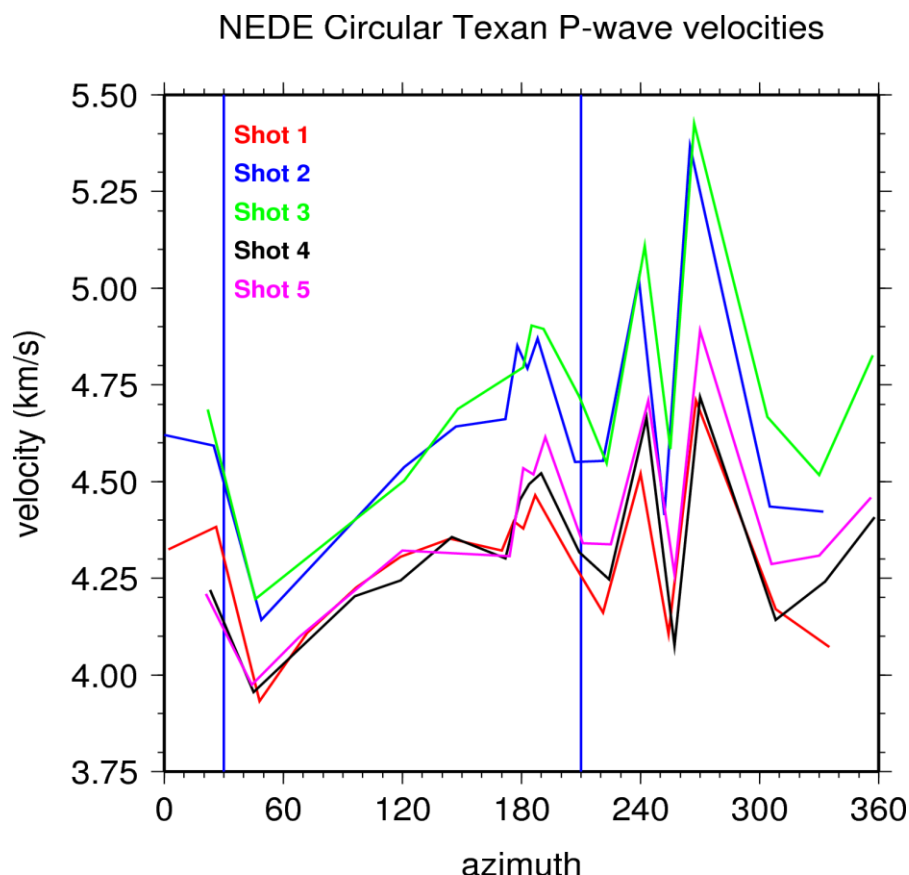
Figure 9. Velocity vs Azimuth for Near-Source Circular Texan Travel-Time Data

(Vertical blue lines indicate azimuth of fast direction from core sample measurements. All other colored lines represent velocity curves for the five shots. The similarity of the curve shapes and that shape's non-conformity to an anisotropic pattern lead us to conclude that these variations in velocity with azimuth are controlled by structural complexities in the near-source region.)

We attempted to see anisotropy in the near-source circular Texan data by plotting the velocity of the first arrival against event-to-station azimuth (Figure 9). Each shot is represented by a different colored line. There is a wide range in P-wave velocities at these stations, but the pattern does not strongly reflect the anisotropy seen in the core samples. The shape of the curves are very similar to each other, leading us to conclude that structural complexities may be causing these variations in velocity. There are several ponds in the path between the shots and some stations, and significant pockets of a schist xenolith were observed in the field. Both of these features could complicate the ray paths and cause velocities to appear erratic. It is possible that the shear-wave velocity model we plan to develop in the future will be more revealing about near-source anisotropy.

In addition, any picking errors are magnified at these short distances. At the near-source stations, a picking error of just 0.02 s can result in a velocity error of 1 km/s. An effort was made to use only high-confidence picks, but this potential source of error should be kept in mind when analyzing the near-source data. Note that this magnified error applies only to the near-source Texans, not the NE and SE linear arrays, which cover larger distances.

3. DETERMINATION OF ATTENUATION PARAMETERS AT LA PAZ, BOLIVIA

3.1 BACKGROUND

The objective of this work is to better understand and account for the attenuation parameters as they relate to the correction of the imprecision uncertainties in global earthquake location.

Introduction

The consequence of a lack of depth phases or phases from a few nearby seismograph stations is mainly that the depths of many events cannot be accurately determined [6]. Further uncertainty in the region of Bolivia is due to the presence of the slab the Nazca plate from the west and a mid-crustal devolvement in the east [6]. Finally, when the seismic stations are not uniformly distributed relative to the epicenter of the event, the estimation of the epicenter of the event may be biased, which in turn biases the depth estimate.

Location needs at least one S phase to control approximately the distance and depth of the hypocenter, but the estimation of the arrival time of an S phase in Bolivia is usually difficult [6].

Effects of attenuation of P and S phase amplitudes are commonly observed in records of some stations of Bolivia network. Errors in the S phase are the most significant and have consequences for the location error.

One common characteristic is a clear phase in the vertical component only, that can be taken as an S phase. However, it is difficult to relate such a single component phase, which does not permit a backazimuth estimate, to a particular earthquake.

This partial or total diminution in amplitude is probably related to the energy lost during the transmission between the focus and the reception

The main case of this energy loss is the complex crustal structure along the path of propagation. The presence of complex crustal structure, composed of interwoven high and low velocity layers as lateral heterogeneities, seems to lead to significant scattering.

Regional Structures and Geology of South America

The main types of structures in South America can be grouped from west to east with several morphological structures composed by rocky formations that have evolved over millions of years. Figure 10 illustrates a general view of the seismic geology of South America. The main types of structures are:

1. Clumps of crystalline Precambrian rocks

2. Basin of deformed Precambrain rocks with a landfill thickness closest to 4000m of Paleozoic rocks, Mesozoic and more recent strata

3. Chains of rocks from different ages folded in forming the Andean Mountain

The South American region can be further represented by the following regional descriptions that include Western Cordillera, Altiplano, Eastern Cordillera and the Chaco-Beniana Plain.

Western Cordillera

This region varies in width from 50 to 90 km west to east; the topography is very chaotic; the eastward contact with the Altiplano is progressive; the Neogene's volcanoes are distributed in the north and in the western mountain chain; the peaks reach altitudes of 4000 to 6350 m in the Altiplano plateau.

Altiplano (Plateau)

This zone is where most of the stations that belong to National Network are located. The region has the following characteristics: the Altiplano begins at 14 ° South where the Western and Oriental mountains of Peru are opened to form an extensive basin and end to the east with the Oriental Mountain. The structural control on the relief in the Altiplano is evident because the anticlines are forming isolated mountains and the synclines agree topographically with valleys in the low zones. The geomorphology that the Altiplano represents is a great tectonic depression that is controlled by blocks that rise and others that sink as much longitudinally as transversely producing a close basin with extensive lagoons in the south and semi salty lakes in the center.

Eastern Cordillera

The Oriental Mountain is the prolongation of the same Oriental chain of Peru that continues towards the south. In Bolivia it is limited in the western part by big faults that separate it from the Altiplano and in the eastern part by the main Frontal Thrust which limits the subandean region. Morphologically, the mountainous countries coincide with structure anticlines which are traversed by river precedents in a juvenile stage of erosion.

Chaco-Beniana Plain

This area of minor altitude with regard to the sea, occupies the major area of the Bolivian east. It is a zone covered with vegetation and recent quaternary sedimentation. There are some outcrops of igneous crystalline rocks of the Precambrian such as in "Cerr Pelado" where the seismological station (SIV) is located.
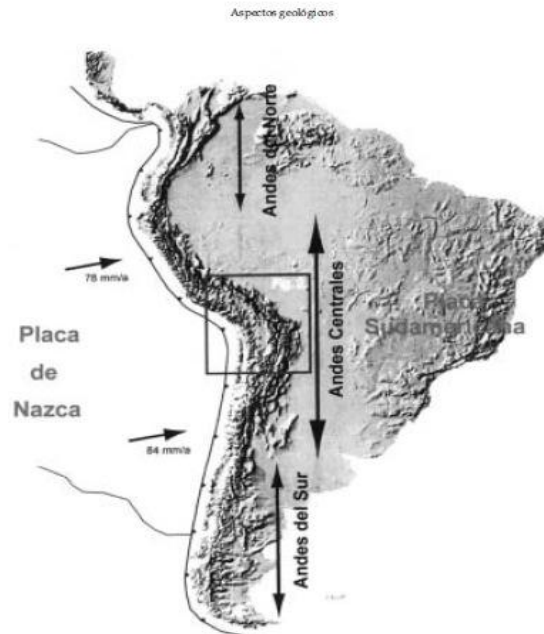
Figure 10. General View of South American Seismic Geology

The Bolivian Network

The seismic Network of Bolivia contains 8 stations, 6 of which are located in the department of La Paz, one in the department of Santa Cruz (SIV) and other one in the department of Potosi (MOC) (see Figure 11).
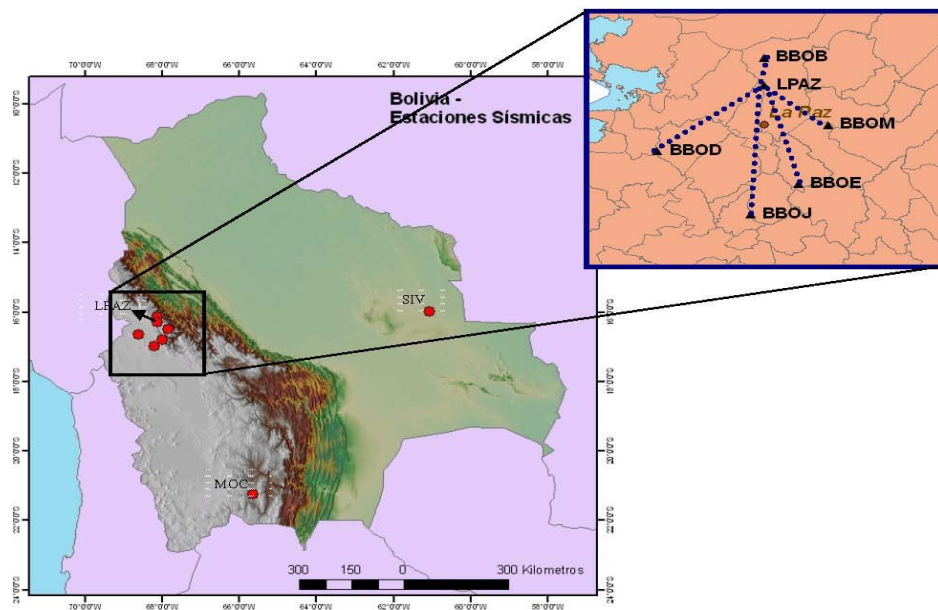
Figure 11. Map of Bolivian Seismic Network

The stations of the National Network are different. The stations in the department of La Paz have a short period and a vertical component while the station LPAZ possesses a broad band

Approved for Public Release; Distribution is unlimited.

sensor with three components. The station located in the department of Santa Cruz (SIV) possesses one long period and one short period. The first period has three components and the second one a vertical component. Finally, the station located to the south of Bolivia, in the department of Potosi, has a sensor with a short period of three components.

The geometric distribution of the stations allows us to have confidence in the location of seismic events but only at a very local level. There continue to be certain limitations in the precision of the calculation of the depth in events of superficial depth (0 – 70 Km).

With regard to the network of stations located in the department of La Paz, we can say that the location and depth calculations of seismic events located inside a radius of 300 km, taking as a center the station LPAZ, give very good results. Table 1 shows the distances between the 6 stations in the La Paz network. This information is to show the area that can affect the signal due to its complex crustal composition and structure.

Table 1. Distance in km Between LPAZ and Surrounding Stations

Estations	LPAZ	BBOB	BBOD	BBOE	BBOJ	BBOM
LPAZ	*	16.23	63.1	60.12	76.25	37.65
BBOB	16.23	*	74.02	76.01	92.41	49.5
BBOD	63.21	74.02	*	68.3	57.16	80.79
BBOE	60.12	76.01	68.3	*	28.52	37.31
BBOJ	76.25	92.41	57.16	28.52	*	63.73
BBOM	37.65	49.5	80.79	37.31	63.73	*

The stations are located in two main deferent's geological environment. Altiplano and Eastern Cordillera. The Altiplano is the highest plate that geomorphology represents a tectonic depression that is controlled by blocks producing a close basin, with extensive lagoons in the south and semi salty lakes in the center as shown in Figure 12.

The La Paz station is located in the Eastern Cordillera where there is a geologic evolution from the lower Ordovician to the present with Hercynian and Andean tectonic deformations. From the lower Triassic to the present granitic intrusions, the Huayna Potosi and Illampu plutonics originate at the top of the Eastern Cordillera. Deformations caused by tectonic Hercynian are evidenced by intense and half-vertical folding with large synclines and anticline structures. Later, the plutonic intrusions deformed the surrounding rocks. The tectonic of the Andes originated both large folds and reverse and transcurrent faults. Each of the three blocks has different features: SW blocks with Silurian outcrops highly folded and faulted on the western edge of the Eastern Cordillera and the central block with the top of the Eastern Cordillera composed of Ordovician sediments and granite plutonic. Folding and fracturing are moderated in the axial and are intense toward edges. The NW limit of LPAZ is the thrust of the Eastern Cordillera.

Figure 12. Geological Map of LPAZ and Stations Around It

(1, BBOB; 2, LPAZ; 3, BOOD; 4, BBOM; 5, BBOE; 6, BBOJ.)

The seismicities in Bolivia that occurred between 2000 and 2009 were earthquakes with intermediate depth. In the eastern area the seismicity was shallow with a few deep earthquakes at the southern end as depicted in Figure 13.
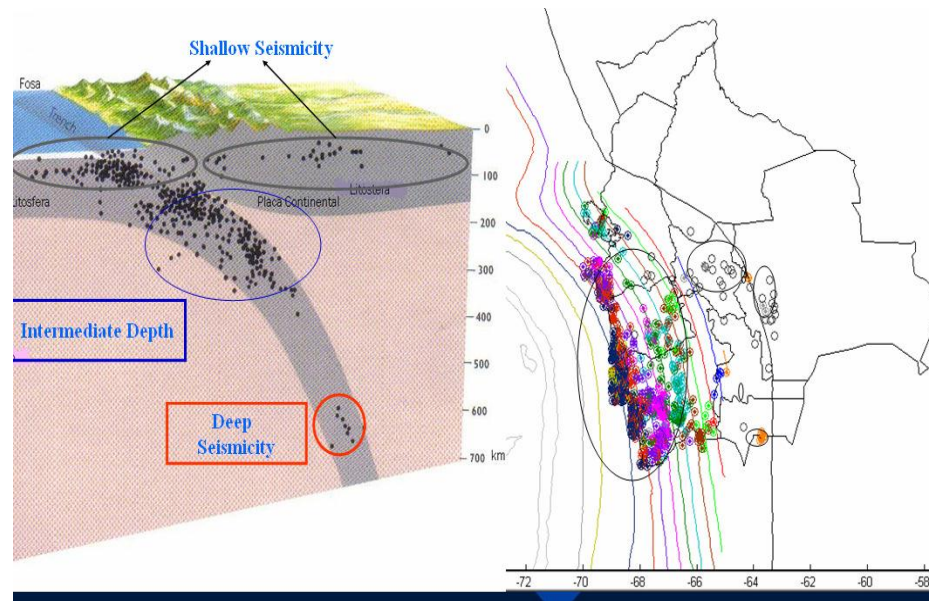
Figure 13. Earthquake Activity from 2000 to 2009 with a Magnitude Ml > 3

(The lines colors correspond to the depth of the Nazca Plate.)

LPAZ station is located in the Eastern Cordillera where there is a geologic evolution from the lower Ordovician to the present with Hercynian and Andean tectonic deformations. From the lower Triassic to the present granitic intrusions, the Huayna Potosi and Illampu plutonics originate at the top of the Eastern Cordillera. Deformations caused by tectonic Hercynian are evidenced by intense and half-vertical folding with large synclines and anticline structures. Later, the plutonic intrusions deformed the surrounding rocks. The tectonic of the Andes originated both large folds and reverse and transcurrent faults. Each of the three blocks has different features: SW blocks with Silurian outcrops highly folded and faulted on the western edge of the Eastern Cordillera and the central block with the top of the Eastern Cordillera composed of Ordovician sediments and granite plutonic. Folding and fracturing are moderated in the axial and are intense toward edges. The NW limit of LPAZ is the thrust of the Eastern Cordillera.

In order to select the data to be analyzed in a given period of time, it was necessary to consider earthquakes at different azimuths and take, as a reference, the LPAZ station. In a first step, earthquakes of each probable seismogenic zone were examined to find those occurring at intermediate and shallow depths as well as those from intraplate and interpolate environments.

3.2 METHODS, ASSUMPTIONS AND PROCEDURES

Localizing Method

In order to estimate accurate source locations, different methods and techniques for locating earthquakes are used at various seismological centers. Some technologies from the past continue to be used to approach the localization of the source. Examples of these techniques include both triangulation of three stations using S-P time difference to get a spatial location of the sources and Wadati diagrams which also need the differences between the S-P arrival times to extrapolate the initial time of the events. Together with the spatial location technique it is

possible to solve the problem that is dependent on four independent variables (three space and one time). However, the solution of this problem is not easy to solve. The locations are also a function of the number of the seismic stations that record the events.

In the present, the methodologies used to locate earthquakes rely on mathematical models based in physics and having many calculations that require the speed of a computational system. The methodologies could be a direct method and an inverse method.

In order to locate earthquakes, we use software based in the Geiger's method with a velocity model of a layer over a semi-infinite space to solve for the hypocenter. The velocities of the first layer is 6.2 km/s for P waves and 3.57 km/s for S waves and the second layer has velocities of 8.2 km/s for P waves and 4.67 km/s for S waves (Figure 14).

The method for locating earthquakes that occur between 0 to 10º (local events) is based on the geometric propagation, taking into account the direct arrival, Pg and Sg phases, or refracted arrival, Pn and Sn. For regional and seleseismic events the location method is based on the travel time tables of the International Association of Seismology and Physics of the Earth's Interior (IASPEI).

The methodology used requires a good spatial distribution of the seismic stations. According to the spatial distribution of our seismic sensors in Bolivia, the control of the event locations is found in its central area. In the location process, with the knowledge of the seismicity of Bolivia, important problems have been identified. The program for intermediate and deep earthquakes (75-350 and 350-700 km depth) ignores that the seismic waves spread through the mantle and that the velocity in this medium is different than that propagated in the crust. This problem results in poor location of the sources and demonstrates that it is necessary to use other phases in order to select both realistic phase tasks and source estimations.
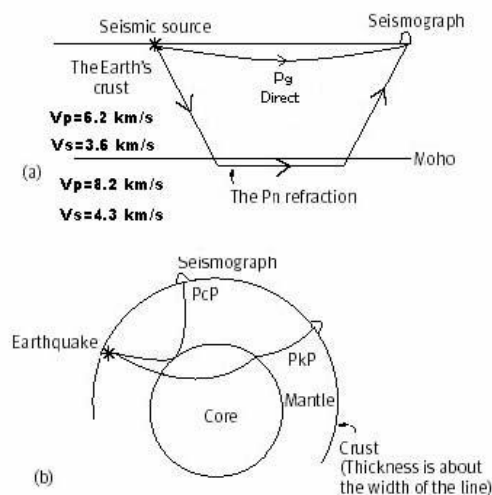
Figure 14. Refracted and Direct Rays from the Seismic Source to Stations

(Propagation into the mantle as reflected in the outer core as well as propagation inside the core).

Crustal Models

The crust models of James [7], Ocola [8], Molina [9] and Zandt [10] work similarly based on two essential parameters: depth and velocities of layers, as well as the arrival times of P and S phases. In all these models the velocity of upper mantle is in the range of $8,0 - 8,2$ km/s. These are the most widely used models. The crust model Wigger [11] is a more complicated model. It also includes lateral variations. Therefore the energies lost in the phases in the different environments cross. The model of Wigger [11] like the other models, has velocities in the upper mantle on the range of $7, 9 - 8,0$ km/s. As seen in Table 2, the experimental crust model has been used at different latitudes but all cases are quite close together. In the end, the results of the various models show little difference.

Table 2. Comparison of Crustal Models

Model	Thickness [km]	Vp	Vs	Layers
James	6	5,0	2,89	
	17	6,0	3,46	
	45	6,7	3,87	
	68	8,0	4,62	3 capas/MI
Ocola	7	4,4	2,54	
	2	6,0	3,46	
	2	5,0	2,89	
	15	6,1	3,52	
	5	6,8	3,93	
	4	6,1	3,52	
	37	6,9	3,98	
	72	8,0	4,62	7 capas/ME
Molina	3	4,9	2,83	
	5	4,2	2,42	
	18	6,0	3,46	
	39	6,9	3,98	
	65	8,2	4,73	4 capas/ME
Zandt	10	5,0	2,89	
	47	6,2	3,58	
	8	7,0	4,04	
	65	8,1	4,68	3 capas/ME
Wigger	4,8	3,8	2,19	
		5,6	3,23	
	17,8	5,5	3,18	
		6,2	3,58	
	4,4	6,8	3,93	
	35,6	6,1	3,52	
	8,3	6,2	3,58	
		7,6	4,39	
	70,9	8,1	4,68	5 capas/ME
General	65	6,2	3,58	
	65	8,0	4,62	3 capas/ME

Data Selection

Direct observation of the seismograms of earthquakes registered for the La Paz station allowed us to detect the same characteristics. These results were then divided into two groups according to their different signals, as shown in Figure 15. In this way, the selection was random.

There are 14 earthquakes of intermediate depth while the others have depth in the crust. The complexity of those in the crust is greater than the intermediate earthquakes. The distances between the stations around LPAZ range from a maximum of 800 km to a minimum of 48 km.
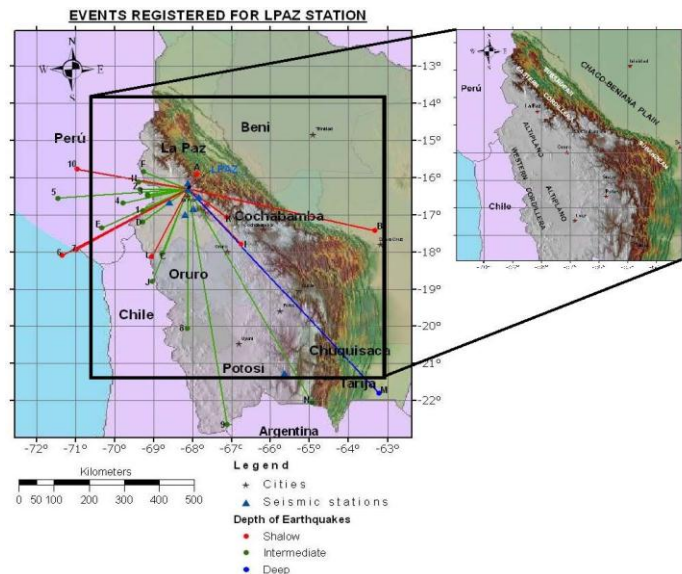
Figure 15. Earthquakes Randomly Selected Using Different Azimuths

The first groups in the above figure are labeled by numbers (1-10) and the other by letters (A-N). The first group of ten earthquakes, 1-10 as seen in Figure 15, recorded in the LPZ or PS08 station are shown in Table 3. The direction and distance are taken from the hypocenter to the LPZ station. The S, Sn or Sg phases are unclear or not recorded in the short period vertical component (SPZ) of LPZ station. They are clear in the broad band in the horizontal component, BHZ, BHN, except for earthquakes 6 and 7. However, the attenuation is present in the P coda for the other earthquakes.

Table 3. Characteristics of First Earthquake Group

No Event	Direction	Depth	Distance (hypocenter-LPAZ station)	Geographic location	Attenuation
1,2,3,4	West	Intermediate	112-182 km	Boundary Peru-Bolivia	P coda and S-SPZ
5	West	Shallow,	350 km	Peru	P coda and S_SPZ
10	West	Intermediate	310km	Peru	P coda
6-7	South-west	Shallow	350,420km	Cost Peru	P wave, and S-SPZ
8	South-East	Intermediate	420km	Bolivia	S –SP z
9	South-East	Intermediate	710 km	Bolivia	P coda

The ray path of most of the earthquakes cross to the north of the Altiplano (a high plateau) while the shallow ones pass through the complex crust. The absence of the S wave or an unclear S wave can give a wrong location and depth, which could be a conduit to a misinterpretation of the data (see Figures 16 and 17).
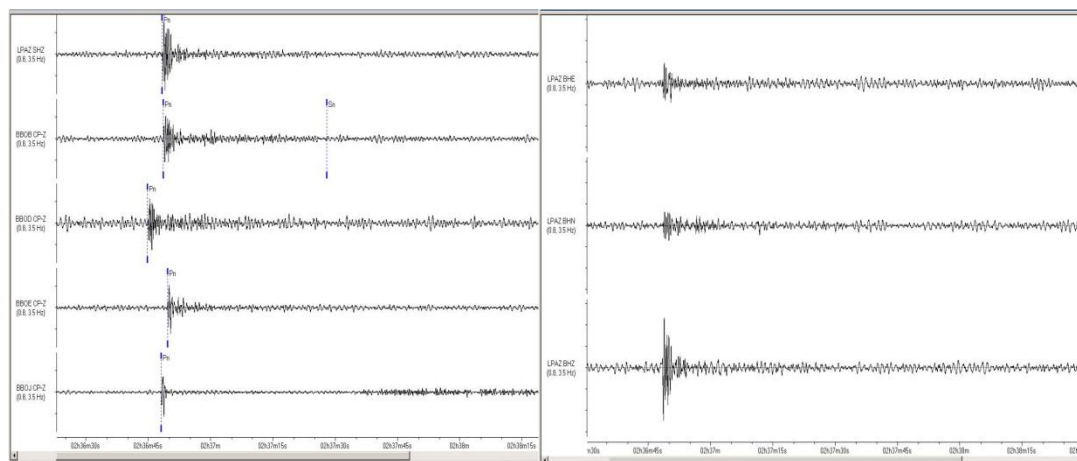
Figure 16. Seismograms of Short Period Vertical Components of LPAZ, BBOJ, BBOB, BBOE

(Short period vertical components on the left; BB three components of LPAZ on the right for 5 earthquakes on Figure 15).
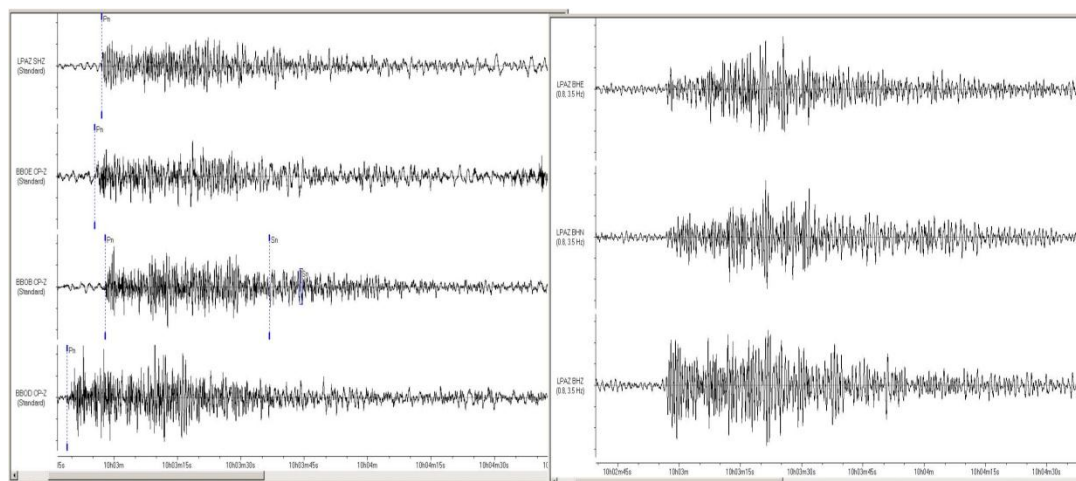
Figure 17. **Seismograms of Short Period Vertical Components of LPAZ, BBOJ, BBOB, BBOE**

(Short period vertical components on the left; BB three components of LPAZ on the right for 7 earthquakes on Figure 15).

The characteristics of the second group of earthquakes, A-M, Figures 18 and 19, also recorded in LPZ or PS08 station are shown in Table 4. The direction and distance are taken from the hypocenter to LPZ station. The S, Sn or Sg phases are clear, in general, in short period

22

vertical component (SPZ) of LPZ station. They are much clearer in broad band components (BBZ), (BHZ and BHN), except for the k earthquake which has the P attenuated. The decay for the P and S waves is very strong.

Table 4. Characteristics of Second Earthquake Group

No Event	Direction	Depth	Distance (hypocenter-LPAZ station)	Geographic location	Attenuation
			LPZ station)		
A	North	Shallow	48km	Bolivia	P and S codes
B	East	Shallow	526km	Bolivia	P and S codes
C,J,L	South-west	Intermediate	205,290,xx	Bolivia	P and S codes
D	South-west	Intermediate	159km	Bolivia	P and S codes
E	South-west	Intermediate	262km	Peru	P and S codes
F,H	North-west	Intermediate	136,130km	Bolivia	P and S codes
I,	South-east	Shallow	220km	Bolivia	P and S codes
K	South-east	Shallow	135km	Bolivia	P attenuated
G	West	Intermediate	112km	Bolivia	P and S codes
N	South-east	Intermediate	xx	Bolivia	P and S codes
M	South-east	Deep		Bolivia	
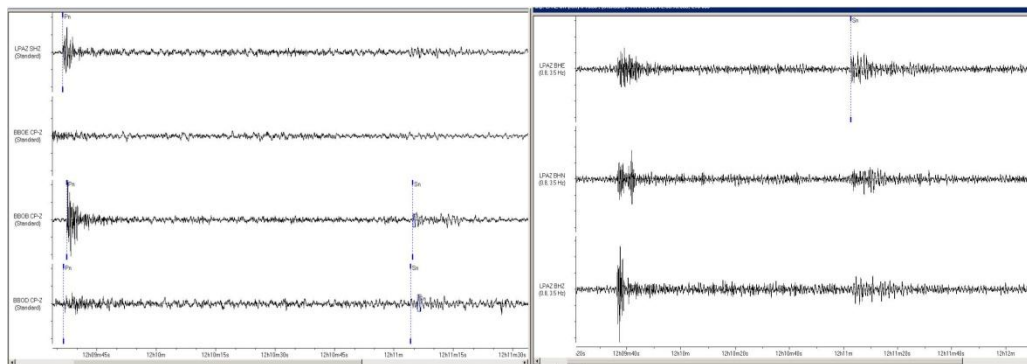
Figure 18. Seismograms of Short Period Vertical Components of LPAZ, BBOJ, BBOB, BBOE

(Short period vertical components on the left; BB three components of LPAZ on the right for M earthquakes on Figure 15. This is a deep earthquake (550km) with clear P and S phases, but attenuation in the code between P and S waves, the Seismogram corresponds to a BB LPAZ station filtered 0.8-3.5 Hz.)
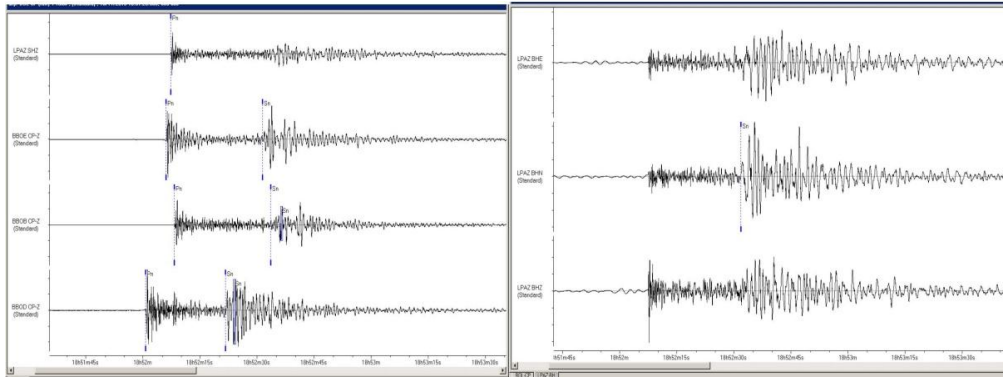
Figure 19. Seismograms of Short Period Vertical Components of LPAZ, BBOJ, BBOB, BBOE

(Short period vertical components on the left; BB three components of LPAZ on the right for D earthquake on Figure 15).

There were 45 earthquakes selected where the S wave did not appear in either the LPZ seismograms or in the BB components. The direct observation of seismograms allowed the division of the 45 earthquakes into two groups. The latitudes of the earthquakes of the first group are located north of 20º with one exception where it is located close to 21˚ (see Figure 20).
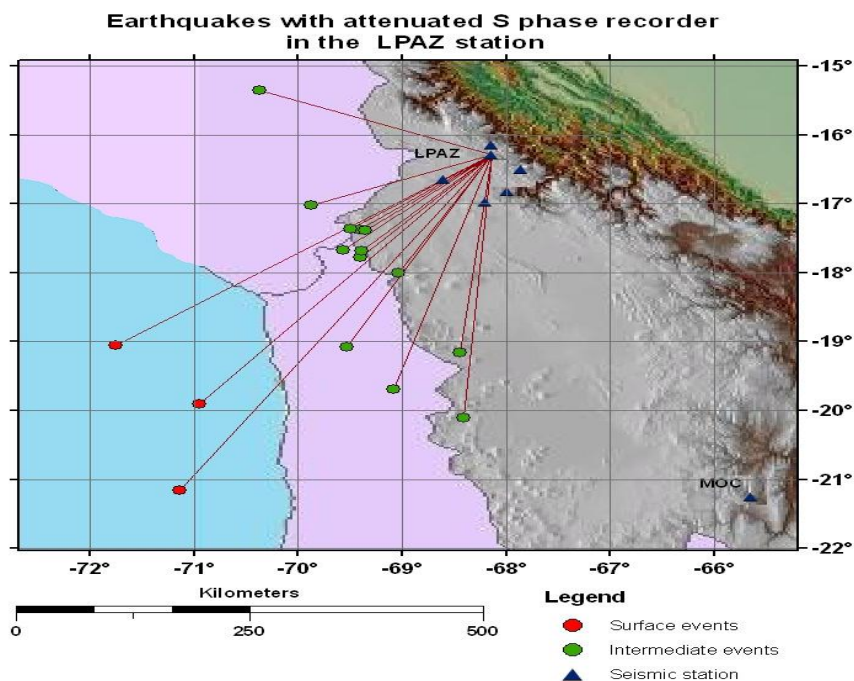
Figure 20. Earthquakes of First Group, Second Selection

These earthquakes have a magnitude Ml greater than 2.5. The shallow earthquakes are located near to the coast while others have an intermediate depth. The maximum distance or

hypocenter for LPAZ station is about 636 km and is located at the west of the LPZ station. The minimum distance for other events is approximately 236 km.

The other earthquakes are found at latitudes 20º and 21º (see Figure 21). None of the earthquakes located have an S wave or an amplitude that is very short. However, in the station MOC, the S wave is clear and an acceptable location of the earthquake is found. The hypocenter distance to the LPZ station averages about 750 km.

The characteristic of both groups allowed proposing a boundary, as seen in Figures 20 and 21, between those groups that could be the two different cases of attenuation. This hypothesis can be confirmed by calculating the factor Q.
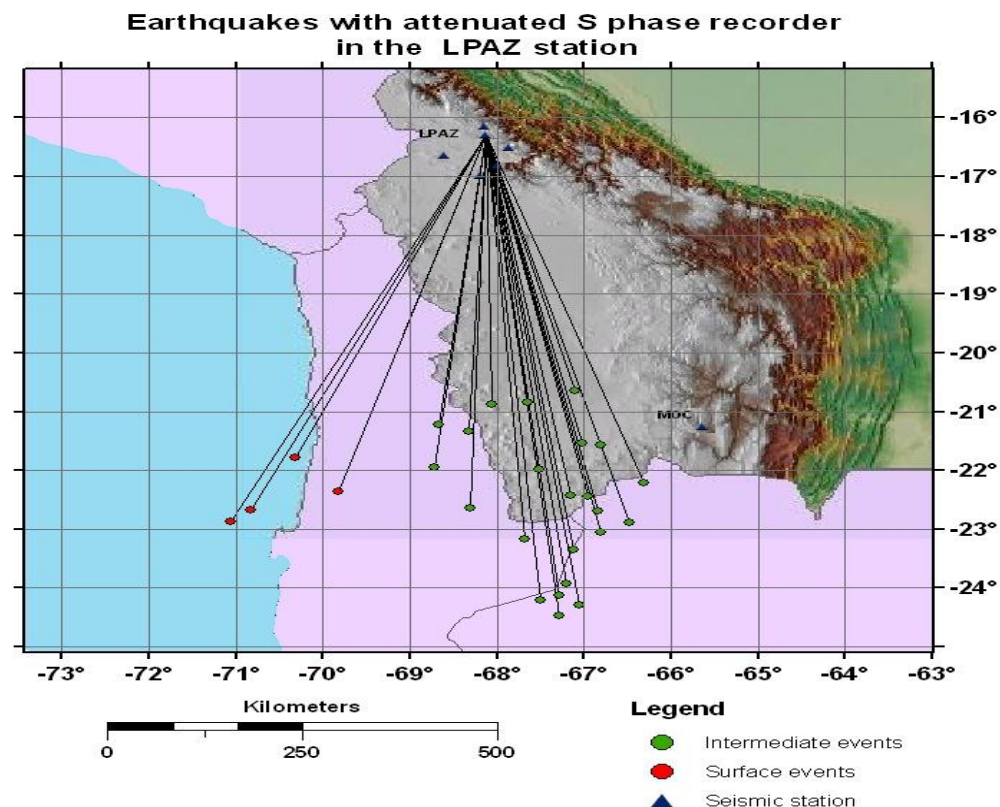
Figure 21. Earthquakes of Second Group, Second Selection - South of the LPAZ Station

The mines around LPAZ station are shown in Table 5. The explosion amount is not enough to produce signals that can be recorded at the LPAZ station.

Approved for Public Release; Distribution is unlimited.

Table 5. Mines Surrounding the LPAZ Station

| MINE	PROVINCIA	Reference
Viloco	Loayza	A 70 Km al SE de la ciudad de La Paz en la Cordillera Tres Cruces
Caracoles	Inquisivi	A 13 Km al NO de Quime
Colquiri	Inquisivi	A 70 Km al Norte de la ciudad de Oruro
Matilde	Camacho	A 155 Km al NW de la ciudad de La Paz
Prov. Polimetálica Berenguela	Pacajes y JM Pando	
Reconquistada	Sud Yungas	A 120 Km de la ciudad de La Paz
Chojlla	Sud Yungas	A 76 Km de la ciudad de La Paz
Bolsa Negra	Sud Yungas	Al SE del Mururata
Chambilaya	Inquisivi	A 4 Km al Sur de Quime
Chicote grande	Inquisivi	

Analysis of Frequency Content

The cutoff frequencies obtained from spectra for the maximum recorded amplitudes for earthquakes are in the range of 2 seconds. The data were taken at the beginning of each P wave recorded at station LPAZ. (Figure 22) The maximum amplitudes obtained correspond to frequencies ranging from 2.0 to 4.0 Hz.. There is no pattern or trend in the graphs to indicate that the predominant frequencies are based on the hypocenter-station distance.
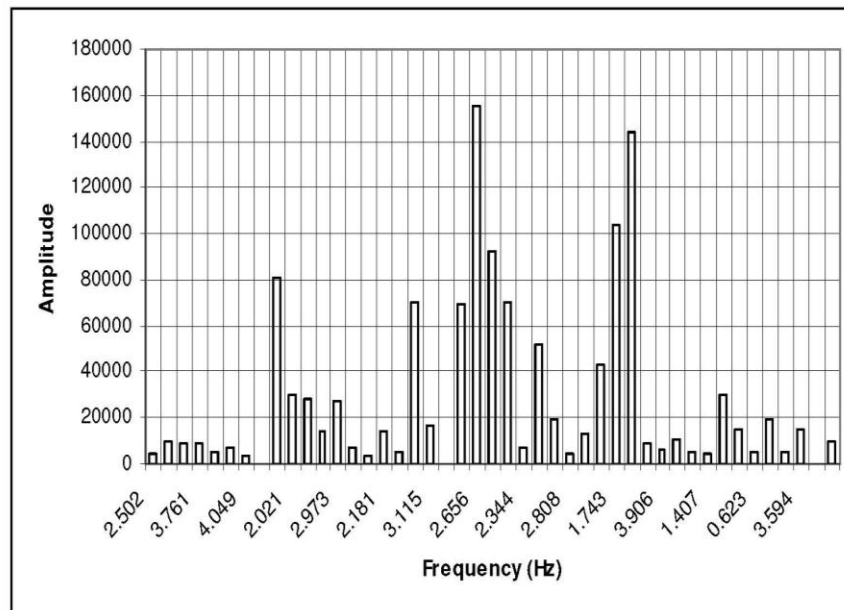
Figure 22. Graphic of Frequency vs Amplitude

The cutoff frequency range between 6.0 and 9.0 Hz, shows a strong decay amplitude. Figure 23a shows the spectrum for an earthquake located at a distance of 216 km from the LPAZ

station, whose cutoff frequency is 7.776 Hz. In figure 23b is the spectrum of an earthquake at a distance of 790 km from the LPAZ station with a cutoff frequency of 8.195 Hz.
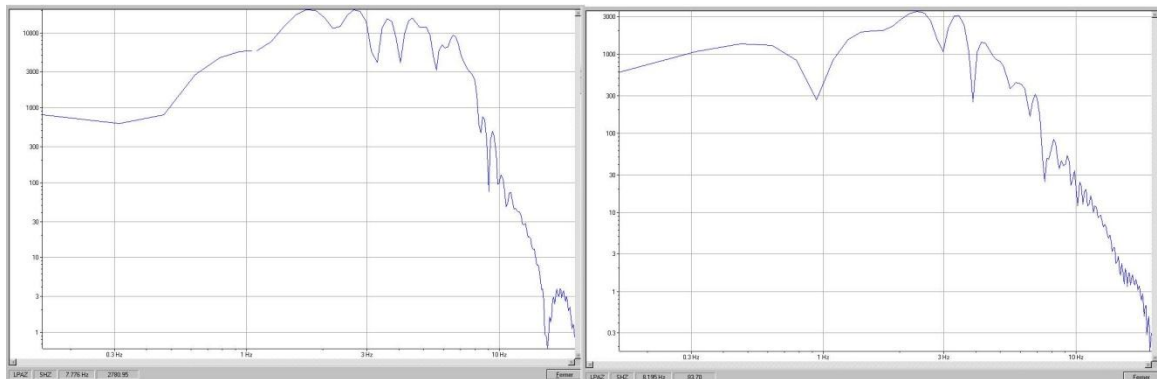
Figure 23. Earthquake Spectrums at 216km and 790 km from LPAZ

(Left panel shows the spectrum 216 km from LPAZ; right panel shows the spectrum 790 km from LPAZ).

These results do not indicate that the cutoff frequency is independent of the distance to the source.

The CODA Q Method

According to the Baumont study [12], Lg phase should have strong attenuation across the Altiplano independent of azimuth propagation. The attenuation will be due more to the scattering of small scale heterogeneities than to the probability of a partial melt in the crustal. This attenuation had a Q value of about 100 at 1 Hz. It was also found that scattering and intrinsic Q are important at 4 Hz. The study was made using a damped squares inversion technique at frequency range 0.6-5 Hz.

Frankel [13] tried to determined how much the observed attenuation in shear waves is due to scattering of small scale heterogeities in the crust versus how much is due to anelasticity. He applied the analysis of the envelopes on high frequency of earthquakes of New York, South Africa and Southern California.

In New York and South Africa he observed an enrichment or high frequency energy that is present in the S and Lg coda which increases as the source receiver distance increases. This implied that scattering in the coda can be detected during its propagation in the crust.

It was observed that when the time of decay at high frequency energy in the coda is compared with the time decay at low frequency, the time decay of the coda is controlled by anelastic attenuation and is insensitive to the scattering attenuation. This is due to the anelastic absorption of production at high frequencies and long distances while the scattering is produced at low frequencies and short distances. The final results of [13] were for New York where the attenuation observed at 15 Hz (distance 100-400 Km) is caused equally by inelasticity and by scattering which is independent of frequency. In South Africa the attenuation is caused by scattering at frequencies of 30Hz. In Southern California the results are unclear. The time decay is very influential in the results.

Havskov [14] tried to determine the frequency dependence in the coda Q values using the time domain coda decay method for sub regions such as the State of Washington. They obtained small variations in the coda Q and the lower coda at St Helen. Q was found with the relation Qc =63f .97 in a band 2-16 Hz.

It was hard to choose the methodology to get the quality Q factor. The principal reason was attenuation which was caused by scattering and intrinsic inelasticity. This leads to a heterogenic crust for the shallow earthquakes and absorption for intermediate depth earthquake.

The analysis of the Q coda may be the best tool for our study. Dainty and Toksoz [15] give a resume for that with the following relation:

$$1/Q= 1/Qi + 1/Qs \qquad (4)$$

where Q is the quality factor obtained by experimental tests on the base of the decay of the seismic wave, Qi is the intrinsic absorption and Qs is the attenuation due to scattering.

By contrast, a high absorption area decreases the scattering process and shortens the duration of the registration. As a result, it can be observed that the coda is affected by attenuation and therefore the recorded coda can estimate the value of attenuation

The measure of Q based on the coda of the wave is identified as Qc. It has been shown in some regions, where the frequencies are above 1.5 Hz, that the Qc estimate is approximately equal to the S wave and identified as Qβ. This is one of the facts supporting the model of the S wave to S wave backscattered. Figure 24 indicates that the decay of the amplitude, called Qc, is due to both relaxation and a scattering attenuation by absorption.
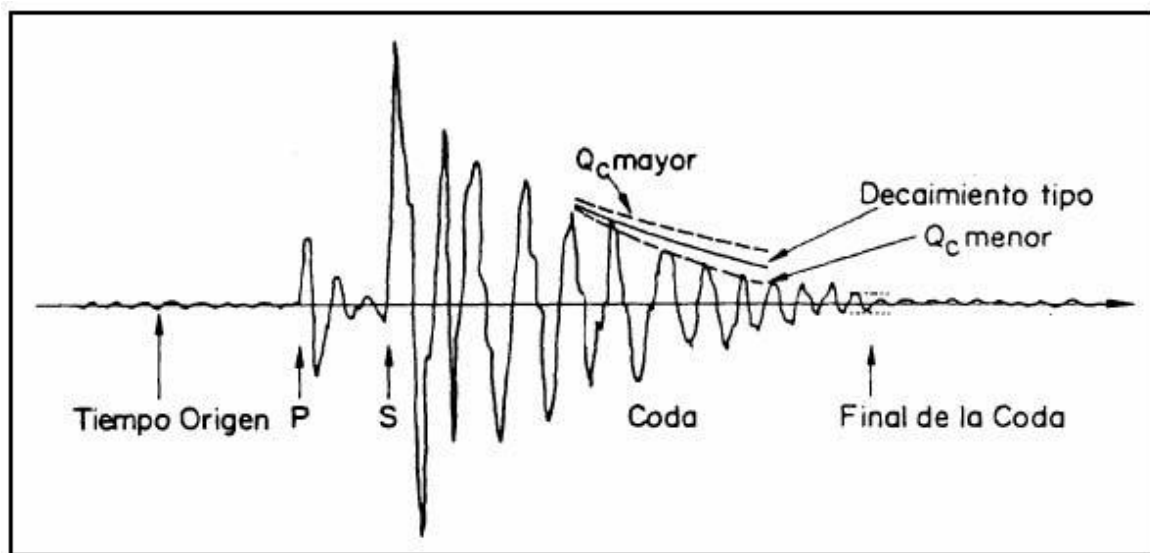

Figure 24. Decay of the Amplitude

Processing

Because it is caused by the combination of the two effects, scattering and anelastic attenuation, the Coda Q method was selected to find the coda attenuation [14] .The characteristics recorded by the seismograms confirmed that aspect and the calculated Q factor caused the effects.

The Q determination from coda wave and shear waves using spectral methods,(Singh et al., 1982) has been demonstrated to be a function of frequency with the form $Q = Qo\ f\alpha$; where α in the range 0.5 to 1.1. Qo and α could showing the variation related to tectonic features.

Dainty [15] suggested that the frequency dependence of coda Q in a range of 1 to 20 Hz is due to scattering while the anelastic attenuation is relatively independent [14]. Aki and Chouet [18] showed that the coda wave amplitude at frequency f, with elapse time t, from the origin can be expressed as:

$$A\ (f,\mathrm{t}) = S(f)\mathrm{t} - \mathrm{ve}^{\ -\pi/t/Q} \tag{5}$$

where $S(f)$ is the source factor, v the geometric spreading parameter (1 for the body wave scattering) and Q the Q wave. Rautian and Khalturin [19] found that this equation is valid only when the lapse time t, is 2 times greater than the Stravel time ts and can be written:

$$\mathrm{Ln}(A(f,\mathrm{t}) + \mathrm{v}\ \mathrm{ln}(\mathrm{t}))=\mathrm{ln}(S(f))-\pi/t/Q$$

$$\tag{6}$$

where $S(f)$ is the source factor, v the geometric spreading parameter (1 for the body wave scattering) and Q the Q wave.

3.3 RESULTS AND DISCUSSION

In order to find the probable attenuation observed in the earthquakes analyzed in this study, software included in the SEISAN program described in Havskov and Ottemoller [20] was applied to located earthquakes. Several earthquakes were tested in a frequency band at 2-16 Hz. The more acceptable results for 4 earthquakes are shown in Figures 25 to 28. Each one corresponds to the selected events. The first earthquake is located south of 20°and 21° latitude with the S wave absent. The results show that the decay code for P wave determined a first value of Q of about 566 at 8Hz frequency (see Figure 25).
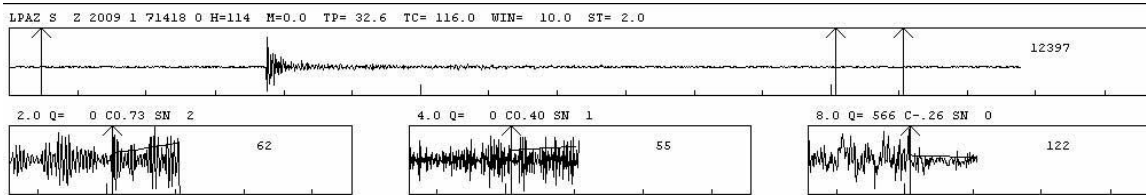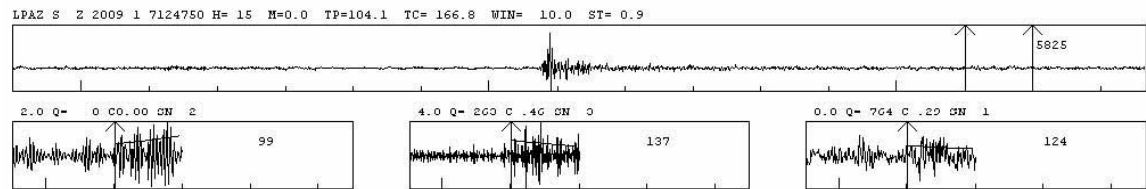
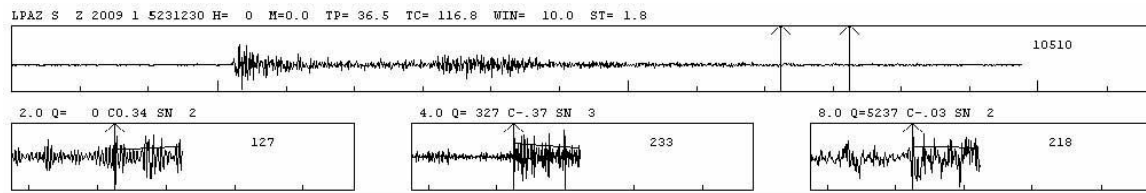Approved for Public Release; Distribution is unlimited.

LPAZ S Z 2009 1 71418 0 H=114 M=0.0 TP= 32.6 TC= 116.0 WIN= 10.0 ST= 2.0

12397

2.0 Q= 0 C0.73 SN 2   62   4.0 Q= 0 C0.40 SN 1   55   8.0 Q= 566 C-.26 SN 0   122

Figure 25

LPAZ S Z 2009 1 7124750 H= 15 M=0.0 TP=104.1 TC= 166.8 WIN= 10.0 ST= 0.9

5825

2.0 Q= 0 C0.00 SN 2   99   4.0 Q= 263 C .46 SN 3   137   0.0 Q= 764 C .29 SN 1   124

Figure 26

LPAZ S Z 2009 1 5231230 H= 0 M=0.0 TP= 36.5 TC= 116.8 WIN= 10.0 ST= 1.8

10510

2.0 Q= 0 C0.34 SN 2   127   4.0 Q= 327 C-.37 SN 3   233   8.0 Q=5237 C-.03 SN 2   218

Figure 27

LPAZ S Z 2010 913 02240 H= 6 M=0.0 TP= 12.9 TC= 45.8 WIN= 10.0 ST= 2.0

1739

2.0 Q= 0 C0.92 SN 1   53   4.0 Q= 162 C-.74 SN 1   37   8.0 Q=2142 C-.13 SN 3   68
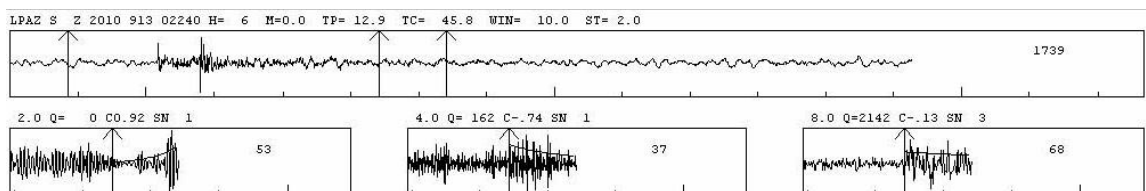
Figure 28

Figures 25-28. Earthquake Results

The second earthquake analysis represents the earthquakes located at southern to 20° and 21° latitude, with S wave clean. This case results in a P wave with a Q value of about 263 at 4Hz.

The third earthquake analyzed has recorded P and S waves so the analysis, with a Q value of 327 at 4 Hz, is ambiguous as shown in Figure 27.

The last one is for earthquakes located near the LPAZ station. Here the Pg and Sg waves are clear and the results show the decay code between the P and S Waves has a Q value of 162 al 4 Hz as shown in Figure 28. This methodology does not consider the depths of the earthquakes.

These first results find the frequencies 4 and 8 Hz. could be the answer. At these frequencies, the envelopes are the best fit for decay amplitude. However, these are only preliminary results and the Q coda was not determined. Finding a lapse time to be used in this calculation was difficult and made use of this method problematic.

Quarry blasts in Bolivia can affect earthquakes. However, due to the low level of explosion in the mine blast and the distance of the mines from the LPAZ station, the effect is minimal at best.

3.4 CONCLUSION

There is no distance dependence for frequencies between 2 and 4 Hz. This does not indicate that the cutoff frequency is independent of the distance to the source. This methodology does not consider the depth of the earthquakes. Our first results, which are approximate, find decay code between P and S Waves where the Q value is 162 at 4 Hz. It is necessary to continue with more studies to obtain a clear Q value. The most acceptable conclusion we can confirm is that the problem with the S wave is due to its attenuation

REFERENCES

[1] Ashby, M.F, and C.G. Sammis, "The Damage Mechanics of Brittle Solids in Compressions," *Pure Appl. GGeophys.*, **133**, 1990, pp. 489-521.

[2] Patton, H., J. Bonner, and I. Gupta, "*Rg* Excitation by Underground Explosions: Insights from Source Modeling the 1997 Kazakhstan Depth of Burial Experiments," *Geophys. J. Int.*, **63**, 2005, pp. 1006-1024.

[3] Stevens, J.L., G.E. Baker, H. Xu, T.J. Bennett, N. Rimer, and S.M. Day, "The physical basis of *Lg* generation by explosion sources," *Proceedings of the 25th Seismic Research Review - Nuclear Explosion Monitoring: Building the Knowledge Base*, LA-UR-03-0629, **1**, 2003, pp. 456-465.

[4] Leidig, M., J. Bonner, J. Britton, K. Murphy, D.T. Reiter, J. Lewkowicz, S. Huffstetler, P. Boyd, R. Martin, D. Murray, A. Garceau, T. Rath, P. West, J. Trippiedi, M. McGinley, A. McGinley, W. Zamora, L. Foley, D. Richter, R. Garfield, A. Martinez, J. Reid, and R. Haas, "*Quicklook: Quantification of Rock Damage from Small Explosions and its Effect on Shear-Wave Generation*," Weston Geophysical Corp. Report, WG-QL0801, 2008.

[5] Stroujkova, A., J.L. Bonner, X. Yang, B.W. Stump, and W. R. Walter, "Source Mechanisms for Explosion in Barre Granite," *Proceedings of the 31st Monitoring Research Review*, Tucson, AZ, 2009.

[6] Drake, A.L. *Estimation of depth and attenuation of earthquakes in Bolivia, Observatorio San Calixto, Bolivia,* Sponsored by U.S. Department of Defense Threat Reduction Agency and Air Force Technical Applications Center Contract No. F49620-97-1-0214, 1996.

[7] James, D.E., "Andean Crustal and Upper Mantle Structure," *J.Geophys. Res.*, **76**, 1971, pp. 3246-3271.

[8] Ocola, L.C. Meyer, R.P. & Aldrich, L.T., Gross crustal structure under Peru – Bolivia Altiplano, *Earthquake Notes*, **42**, 1971, pp. 33-48.

[9] Molina, W., "Estructura de los Andes Centrales a Través de Residuos y Atenuación de Ondas Sísmicas," *Tesis de Grado,* UMSA, Facultad de Ciencias Puras y Naturales, Departamento de Geociencias, La Paz – Bolivia, 1977.

[10] Zandt, G., S.L. Beck, S.R. Ruppert, C.J. Ammon, D. Rock, E. Minaya, T.C. Wallace and P.G. Silver, "Anomalous Crust of the Bolivian Altiplano, Central Andes: Constraints from Broadband Regional Seismic Waveforms," *Geophyisical Research Letters,* **23**, 1996, 11.

[11] Wigger, P.J., M. Schmitz, M. Araneda, G. Asch, S. Baldzuhn, P. Giese, W.-D.Heinsohn, E. Martinez, E. Ricaldi, P. Röwer and J. Viramonte, "Variation in the Crustal Structure of the Southern Central Andes Deduced from Seismic Refraction Investigations," *In Tectonics of the*

Southern Central Andes (K,-J, Reutter, E, Scheuber and P,J, Wigger, eds), Springer-Verlag, Berlin, 1994, pp. 23-48.

[12] Baumont, D., A. Paul, S. Beck and G. Zandt, "Strong Crustal Heterogeneity in the Bolivian Altiplano as Suggested by Attenuation of Lg Waves," *J. Geophys. Res.*, **104**, 1999, pp. 20287-20305.

[13] Frankel, A., "Mechanisms of Seismic Attenuation in the Crust: Scattering and Anelaticity in New York, State, South Africa and Sourthern California," *J. Geophys. Res.,* **96**, 1991, pp. 6269-6289.

[14] Havskov, J., S. Malone, D. McClurg, and R. Crosso, "Coda Q for the State of Washington, Bull.," *Seim. Soc. Am.*, **74**, 1989, pp. 1024-1038.

[15] Dainty, A.M., and Toksoz, M.N., "Seismic Codas on the Earth and the Moon: A Comparison," *Phys. Earth and Plan. Int.,* **20**, 1981, pp. 250-260.

[16] Singh, S.K., R.J. Aspel, J. Fried, and J.N. Brune, "Spectral Attenuation of SH Waves Along the Imperial Fault," *Bull. Seim. Soc. Am.,* **72**, 1982, pp. 2003-2016.

[17] Dainty, A., "A Scattering Model to Explain Seismic Q Observations in the Lithosphere Between 1 to 30 Hz," *Geophys. Res. Lett.* **11**, 1981, pp. 1126-1128.

[18] Aki, K., and B. Chouet, "Origin of coda waves: source attenuation of Scattering effects," *J. Geophys. Res.* **80**, 1975, pp. 3322-3342.

[19] Rautian, T.G., and V.I. Khalturin, "The Use of the Coda for Determination of the Earthquake Source Spectrum," *Bull. Seism. Soc. Am.*, **68**, 1987, pp. 923-948.

[20] Havskov, J. and Ottemoller, "SEISAN Earthquake Analysis Software," *Seismological Research Letters,* **70**, 2000, pp. 532-534.

DISTRIBUTION LIST

DTIC/OCP
8725 John J. Kingman Rd, Suite 0944
Ft Belvoir, VA 22060-6218   1 cy

AFRL/RVIL
Kirtland AFB, NM 87117-5776   2 cys

Official Record Copy
AFRL/RVBYE/Robert Raistrick   1 cy